2. Taillefer R, Robiduox A, Lambert R, Turpin S, LaPerriere J. Technetium-99m-sestamibi prone scintimammography to detect primary breast cancer and axillary lymph node involvement. *J Nucl Med* 1995;36:1758–1765.
3. Kao CH, Wang SJ, Liu TJ. The use of technetium-99m methoxyisobutylisonitrile breast scintigraphy to evaluate palpable breast masses. *Eur J Nucl Med* 1994;21:432–435.
4. Okada RD, Glover D, Gaffney T, Williams SJ. Myocardial kinetics of technetium-99m-hexakis-2-methoxy-2-methylpropsyl-isonitrile. *Circulation* 1988;77:491–498.
5. Mousa S, Cooney J, Williams SJ. Relationship between regional myocardial blood flow and the distribution of ^{99m}Tc-sestamibi in the presence of total coronary artery occlusion. *Am Heart J* 1990;119:842–847.
6. Piwnica-Worms D, Kronauge JF, Chiu ML. Uptake and retention of hexakis(2-methoxyisobutylisonitrile) technetium (I) in cultured chick myocardial cells: mitochondrial and plasma membrane potential dependence. *Circulation* 1990;82:1826–1838.
7. Crane P, Laliberti R, Heminway S, Thoalen M, Orlandi C. Effect of mitochondrial viability and metabolism on Tc-99m sestamibi myocardial retention. *Eur J Nucl Med* 1993;20:20–25.
8. Horaker, Russel L, Klenk N. Angiogenesis, assessed by platelet/endothelial cell adhesion molecule antibodies, an indicator of node metastases and survival in breast cancer. *Lancet* 1992;340:1120–1124.
9. Visscher DW, DeMattia F, Ottosen S, Sarkar FH, Crissman JD. Biologic and clinical significance of basic fibroblast growth factor immunostaining in breast carcinoma. *Modern Pathol* 1995;8:665–670.
10. Diggles L, Mena I, Khalkhali IJ. Technical aspects of prone dependant breast scintimammography. *J Nucl Med Technol* 1994;22:165–170.
11. Khalkhali I, Cutrone JA, Mena IG, et al. Scintimammography. The complementary role of Tc-99m sestamibi prone breast imaging for the diagnosis of breast carcinoma. *Radiology* 1995;196:421–426.
12. Weidner N, Semple JP, Welch WR, Folkman J. Tumor Angiogenesis and metastasis-correlation in invasive breast carcinoma. *NEJM* 1991;324:1–8.
13. Weidner N, Folkman J, Pozza F, et al. Tumor angiogenesis: a new, significant, and independent prognostic indicator in early-stage breast carcinoma. *J Natl Cancer Inst* 1992;340:1875–1887.
14. Obrenovitch A, Monsigny M. Angiogenese tumorale. *Pathol Biol* 1986;34:189–201.
15. Scopinaro F, Schillaci O, Scarpini M, et al. Technetium-99m-sestamibi: an indicator of breast cancer invasiveness. *Eur J Nucl Med* 1994;21:984–987.
16. Hove M, Leonard MH, Villanueva-Mayer J, Cowan DF. Histopathologic correlates of ^{99m}Tc-sestamibi scanning in the breast [Abstract]. *Modern Pathol* 1995;19A.

Fluorine-18-Fluorodeoxyglucose PET Versus Thallium-201 Scintigraphy Evaluation of Thyroid Tumors

Hidemasa Uematsu, Norihiro Sadato, Toshio Ohtsubo, Tatsuro Tsuchida, Satoshi Nakamura, Katsuya Sugimoto, Atsuo Waki, Norio Takahashi, Yoshiharu Yonekura, Gota Tsuda, Hitoshi Saito, Nobushige Hayashi, Kazutaka Yamamoto and Yasushi Ishii
Department of Radiology, Biomedical Imaging Research Center, and Department of Otolaryngology, Fukui Medical School, Fukui, Japan

To determine whether PET could help differentiate malignant from benign thyroid tumors, ^{18}F-fluorodeoxyglucose (FDG) accumulation and ^{201}Tl scintigraphy were examined relative to histological diagnosis. **Methods:** Nodular thyroid lesions in 11 patients were evaluated before surgical resection. Static PET scanning with 370 MBq FDG was done for 20 min (from 40 to 60 min postinjection) in all patients, and standardized uptake values (SUVs) in these lesions were calculated. In addition, eight patients were evaluated with dynamic PET scan up to 60 min postinjection, and the lesions were further evaluated using graphical analysis. Thallium-201 delayed images were visually evaluated in 10 patients. **Results:** Four of 11 nodules were well-differentiated papillary carcinoma, another five were benign follicular adenomas, one was a multinodular goiter and another a case of chronic thyroiditis that was proved not to contain a nodule. Time-activity curves of FDG uptake showed different patterns in malignant and benign tumors. In the malignant tumors, FDG uptake increased with time after the tracer injection. By contrast, FDG uptake in benign tumors gradually decreased. With use of a cutoff value of 5.0 mg/ml for SUV and 10 $\mu l \cdot min^{-1} \cdot ml^{-1}$ for Kc (K complex value determined using the linear fitting of the time-activity curve of FDG accumulation), all of the four malignant nodules and the six benign nodules were separated correctly. Chronic thyroiditis had high SUV in the malignant range. Of the four patients with thyroid carcinoma, the delayed ^{201}Tl images revealed a slightly higher or equal uptake to background activity. In a patient with chronic thyroiditis, the delayed ^{201}Tl images revealed diffuse accumulation higher than background activity. **Conclusion:** FDG-PET is superior to ^{201}Tl in differentiating malignant from benign tumors. Both SUVs and Kc values were useful indexes for this discrimination. Although careful evaluation is needed for chronic inflammatory lesions, this technique appears to be useful in evaluating thyroid nodules.

Key Words: thyroid tumors; PET; thallium-201 scintigraphy; fluorine-18-fluorodeoxyglucose

J Nucl Med 1998; 39:453–459

Because surgical resection is the effective treatment for thyroid tumors, preoperative differentiation between malignant and benign nodules is essential. Thyroid tumors are usually evaluated before surgery by means of clinical examination, sonography, computed tomography (CT) and fine-needle aspiration biopsy (*1*).

Sonography is generally the first choice for the evaluation of thyroid morphology because of its sensitivity for small nodule detection (*1*). The combination of sonography and fine-needle aspiration biopsy is routine in many centers. The sensitivity and specificity of scintigraphy with solitary thyroid nodules were 100% and 5.5%, respectively, whereas those of fine-needle aspiration biopsy were 100% and 91.2%, respectively (*2*).

In spite of these attributes, fine-needle aspiration biopsy has limitations. Accuracy depends on the skill and experience of the operator and the cytopathologist. Some benign adenomas are difficult to distinguish from malignancies (*3*). Follicular adenomas are particularly difficult to distinguish from well-differentiated follicular cancer. This distinction is made on the basis of whether there is capsular invasion and is difficult even on permanent histopathological sections. To improve diagnostic accuracy further, additional methods of evaluation are needed.

Although conventional radiography such as CT scanning and magnetic resonance imaging (MRI) can sometimes be used effectively, it often cannot accomplish clear, quick determina-

Received Dec. 23, 1996; revision accepted Jun. 12, 1997.
For correspondence or reprints contact: Hidemasa Uematsu, MD, Department of Radiology, Fukui Medical School, 23 Shimoaizuki, Matsuoka-cho, Yoshida-gun, Fukui, Japan, 910-11.

TABLE 1
Summary of Clinical and Imaging Data of Patients with Thyroid Lesions

Patient no.	Age (yr)	Sex	Pathological diagnosis	Size (cm)	SUV (mg/ml)	Kc ($\mu l \cdot min^{-1} \cdot ml^{-1}$)	^{201}Tl delayed image
1	48	F	Papillary carcinoma	1.5	7.06	27.66	(+)
2	67	M	Papillary carcinoma	5.1	6.62	27.87	(+)
3	53	M	Papillary carcinoma	1.8	16.89	83.77	(+)
4	47	F	Papillary carcinoma	1.8	5.69	24.00	(+)
5	58	F	Follicular adenoma	2.2	0.96	na	(+)
6	47	F	Follicular adenoma	2.1	1.66	na	na
7	67	F	Follicular adenoma	1.5	2.17	6.47	(−~+)
8	67	F	Follicular adenoma	3.5	2.92	7.97	(+)
9	36	M	Follicular adenoma	1.5	1.74	9.36	(+)
10	36	F	Multi[illegible]ular goiter	†	4.34	na	(+)
11	58	F	Chro[illegible]hyroiditis	*	6.30	28.73	(+)

*No apparent nodules.
†Multiple nodular components.
SUV and Kc are average values; + = a nodule with ^{201}Tl uptake only slightly higher than or equal to background activity; − = a nodule with ^{201}Tl uptake lower than background activity; na = not available.

tion of whether a lesion is malignant. CT scanning and MRI provide excellent anatomic detail for evaluation of such lesions and allow for the accurate assessment of the extent of the thyroid lesions and soft-tissue involvement, but these techniques are still limited in their ability to facilitate a distinction between certain malignant and benign thyroid lesions.

Various radioisotopes such as ^{99m}Tc-pertechnetate, ^{123}I, ^{201}Tl and ^{99m}Tc-methoxyisobutylisonitrile (MIBI) are used to detect primary thyroid tumors. Technetium-99m-pertechnetate is inexpensive and readily available from on-site generators. However, most primary thyroid nodules are shown as cold spots on ^{99m}Tc-pertechnetate scans; hence, no specific diagnosis for malignancy can be made.

Iodine-123 is cyclotron produced and is considerably more expensive than ^{99m}Tc-pertechnetate. Most primary thyroid nodules also are shown as cold spots in iodine scans. Although whole-body ^{123}I or ^{131}I scintigraphy is highly specific for detecting recurring local tumors and metastases after surgery, these scintigraphs need a prolonged period of thyroid hormone withdrawal, restriction of dietary iodine intake, repeated patient visits and administration of a relatively high radiation dose. If preparative thyroid hormone withdrawal is not done completely, radioiodine may not accumulate on a recurring local tumor or metastases after surgery, even if the tumor is a well-differentiated cancer. Images obtained with both ^{99m}Tc-pertechnetate and ^{123}I yielded essentially the same information, and the differences between iodine and technetium images are small (*4*).

Technetium-99m-MIBI was originally introduced as a myocardial perfusion imaging agent that has been reported to accumulate in benign and malignant lesions such as lung (*5,6*) and parathyroid tumors (*7,8*). Whereas accumulation of ^{99m}Tc-MIBI is useful in evaluating metastases or predicting recurrence, in differentiating malignant from benign thyroid tumors ^{99m}Tc-MIBI proves insufficient (*9*).

Today, ^{201}Tl scintigraphy could be of major clinical use to differentiate malignant from benign nodules (*10–12*). Tonami et al. (*10*) introduced ^{201}Tl scintigraphy as a tool for detecting malignant lesions of the thyroid. Thallium-201 scintigraphy could be of major clinical use to differentiate malignant from benign nodules (*10–12*), and delayed scanning has been reported to be useful (*11*). Thyroid nodules that accumulated ^{201}Tl in early scans and revealed no significant decrease in ^{201}Tl activity in delayed scans were all malignant. Thallium-201 is more sensitive than ^{131}I (diagnostic) for detecting differentiated thyroid carcinoma, even during the euthyroid state (*13*). Therefore, ^{201}Tl is widely used to differentiate malignant from benign

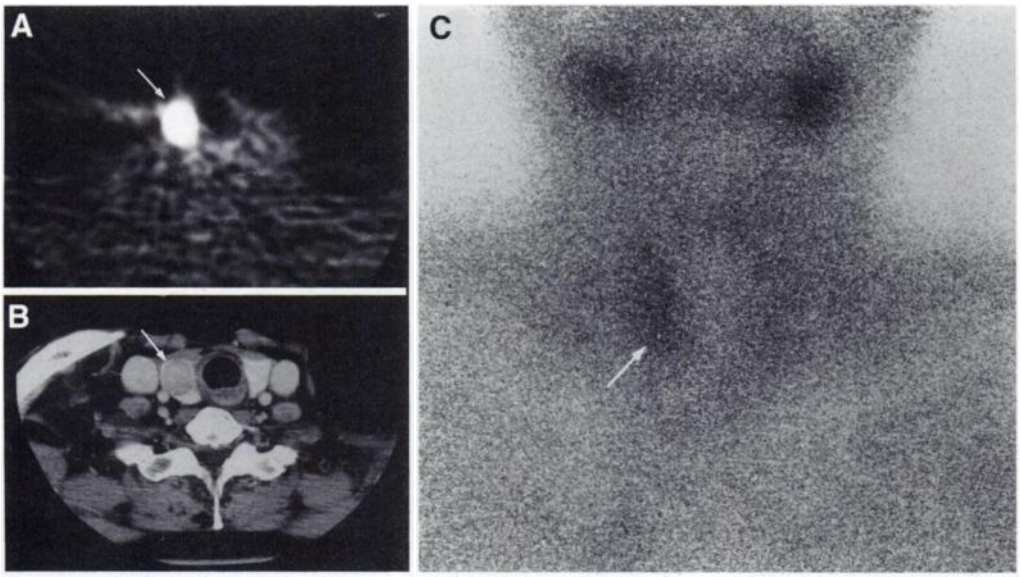

FIGURE 1. A 53-yr-old man with a tumor in the right lobe of the thyroid. This tumor was surgically resected and histological diagnosis was papillary carcinoma. (A) FDG-PET shows markedly increased uptake in the tumor (white arrow, SUV: 16.89 mg/ml, Kc: 83.77 μl/min/ml). (B) On the corresponding CT image, the thyroid tumor was present in the right lobe (white arrow). (C) On the delayed ^{201}Tl scintigraphic image, ^{201}Tl uptake was higher than background activity (white arrow, +).

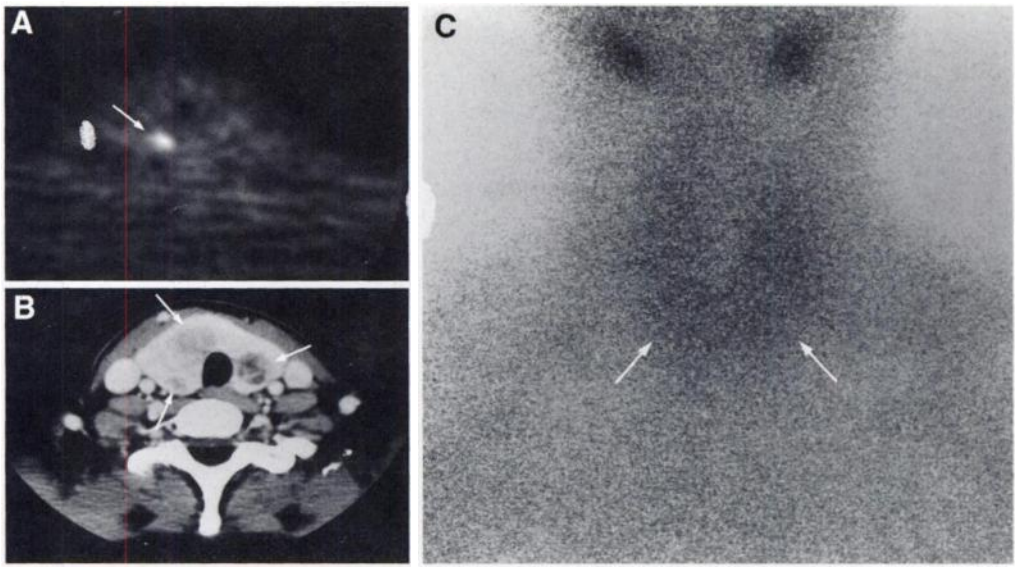

FIGURE 2. A 36-yr-old woman with multiple nodular components in the thyroid. Histological diagnosis was multinodular goiter. (A) FDG-PET shows increased uptake in one nodule (white arrow, SUV: 4.34 mg/ml). (B) On the corresponding CT image, multiple nodular components were present in the thyroid (white arrows). (C) On the delayed ^{201}Tl scintigraphic image, ^{201}Tl uptake was equal to background activity (white arrows, +).

thyroid nodules. However, various benign tumors such as adenomas, multinodular goiter and chronic thyroiditis were also positively delineated by ^{201}Tl (*10*).

Recently, FDG-PET has become an established technique for assessing tissue glucose metabolism in vivo. FDG-PET seems to be highly sensitive in detecting extracranial head and neck neoplasms (*14–20*). FDG-PET has been used as a screening test in patients suspected of head and neck squamous cell carcinomas (*14*). The detection of recurrent head and neck carcinoma is feasible with FDG-PET (*15*). FDG-PET is highly sensitive in evaluating the lymph node metastases of malignant neck tumors (*16*). The response of head and neck tumors to radiation can be evaluated using FDG-PET (*17–19*). FDG-PET is a useful method for observation of therapeutic measures in patients undergoing systemic chemotherapy (*19*).

Adler and Bloom (*21*) and Bloom et al. (*22*) evaluated FDG uptake in primary thyroid tumors. They showed that the FDG uptake successfully discriminated between benign and malignant tumors. In a recent study, Feine et al. (*23*) reported that a combination of FDG and ^{131}I whole-body imaging enabled the detection of local recurrence or metastases. Feine et al. (*23*) and Grünwald et al. (*24*) reported that in highly differentiated tumors, ^{131}I scintigraphy had a high sensitivity, whereas in poorly differentiated carcinomas FDG-PET was superior.

The purpose of this study was to evaluate the usefulness of FDG-PET in differentiating malignant from benign thyroid gland nodules relative to ^{201}Tl.

MATERIALS AND METHODS

Subjects

Eleven patients (8 women, 3 men; age range 36–67 yr) were examined using FDG-PET. Nodular thyroid lesions of these patients were evaluated using CT scanning, ^{201}Tl scintigraphy and FDG-PET. Of these 11 patients, 9 had solitary thyroid nodules, 1 had a multinodular goiter and 1 had chronic thyroiditis, which, through clinical examination, was suspected to contain a nodular lesion. The maximum diameters of the tumors on CT scans ranged from 1.5 to 5.1 cm. In the patient with multinodular goiter, there were multiple nodular components. Patients with diabetes mellitus were not included in this study.

CT Scanning

CT scans were obtained on all patients. Using a standard commercial CT system (High Speed Advantage RP scanner, GE-YMS, Tokyo, Japan), we obtained contiguous transaxial images (field of view [FOV] 23 × 23 cm; matrix size 512 × 512) with a peak kilovoltage of 120 and a tube current of 250 mAs from the thoracic inlet to the base of the skull at 7-mm intervals and with

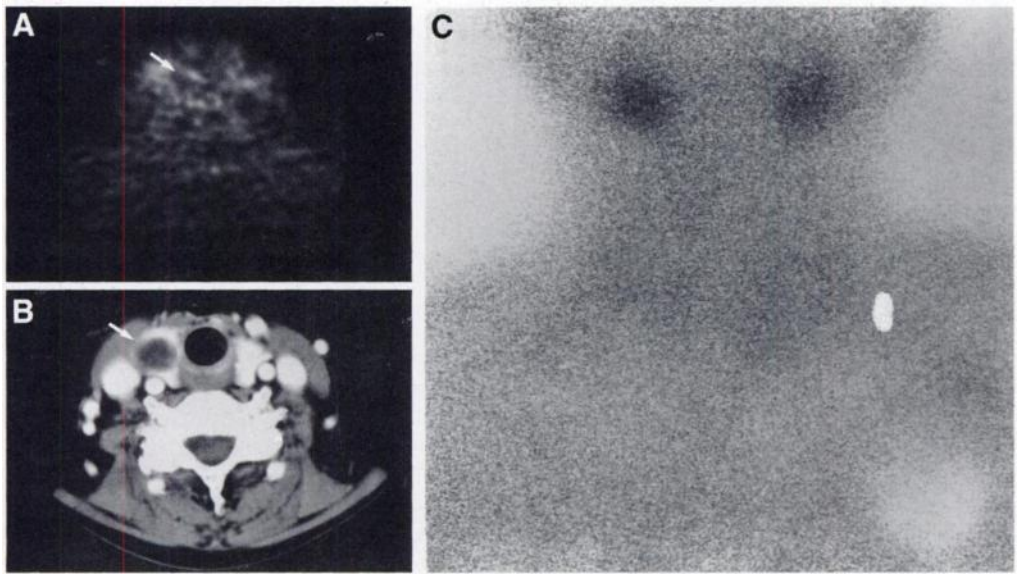

FIGURE 3. A 67-yr-old woman with a tumor in the right lobe of the thyroid. This tumor was surgically resected, and the histological diagnosis was follicular adenoma. (A) On the FDG-PET image, there is no visual evidence of FDG uptake in the tumor (white arrow; SUV: 2.17 mg/ml; Kc: 6.47 $\mu l \cdot min^{-1} \cdot ml^{-1}$. (B) On the corresponding CT image, the thyroid tumor was present in the right lobe (white arrow). (C) On the delayed ^{201}Tl scintigraphic image, ^{201}Tl uptake was equal to background activity (+).

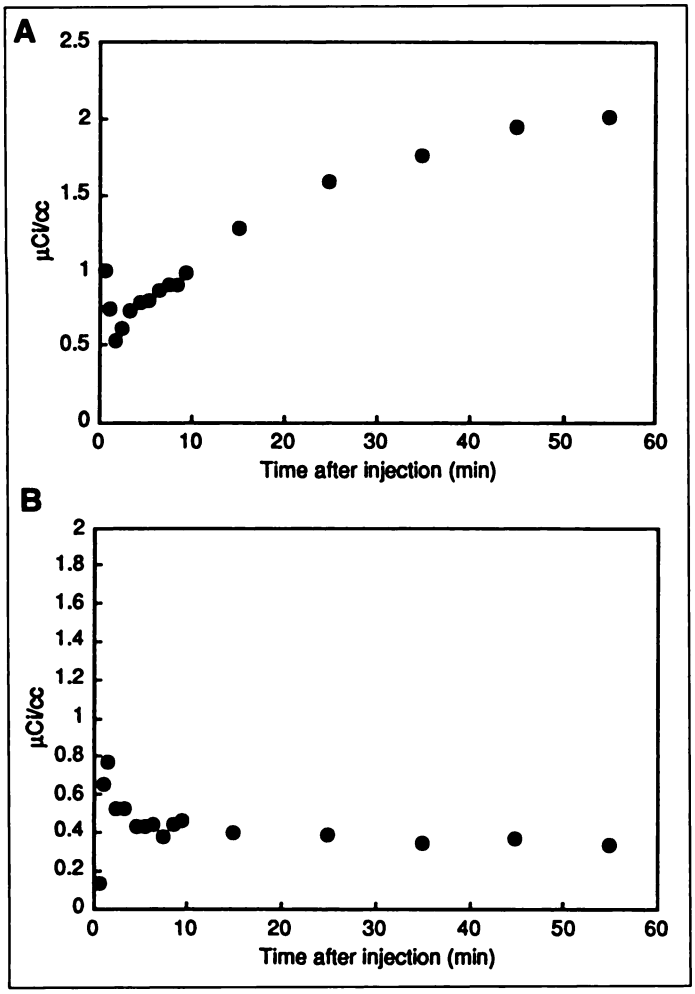

FIGURE 4. (A) Typical time-activity curve of FDG uptake of the papillary carcinoma (same patient as in Fig. 1). FDG uptake increased with time after the tracer injection. (B) Typical time-activity curve of FDG uptake of the follicular adenoma (same patient as in Fig. 2). FDG uptake of a follicular adenoma gradually decreased with time after the tracer injection.

7-mm collimation. For contrast enhancement studies, 100 ml of contrast material (lopamidol 300 mg/ml, Nihon Schering, Osaka, Japan, or lohexol 300 mg/ml, Daiichi Seiyaku, Tokyo, Japan) was injected intravenously as a bolus in all patients.

PET Scanning

All patients underwent FDG-PET study after a 4-hr fast. FDG-PET was performed using a high-resolution, whole-body PET scanner with an 18-ring detector arrangement (Advance, GE-YMS, Tokyo, Japan). The physical characteristics of this scanner have been described in detail by DeGrado et al. (*25*). Briefly, the system permits the simultaneous acquisition of 35 transaxial images with an interslice spacing of 4.25 mm. Both axial and transaxial resolution are 4.2 mm, allowing multidirectional reconstruction of the images without loss of resolution. The FOV and the pixel size of the reconstructed images were 256 and 2 mm, respectively. A 10-min transmission scan was acquired with a $^{68}Ge/^{68}Ga$ source for attenuation correction. Approximately 370 MBq FDG was injected intravenously, and static scanning was performed for 20 min (40–60 min postinjection) in all patients. In addition, eight patients were evaluated using dynamic PET images up to 60 min postinjection. The mode of dynamic data acquisition consisted of four 30-sec frames, eight 60-sec frames and five 600-sec frames. In the eight patients who received dynamic scans, the last two frames (40–60 min postinjection) of the dynamic acquisition were used to obtain the static image for analyzing FDG uptake in the tumor. The

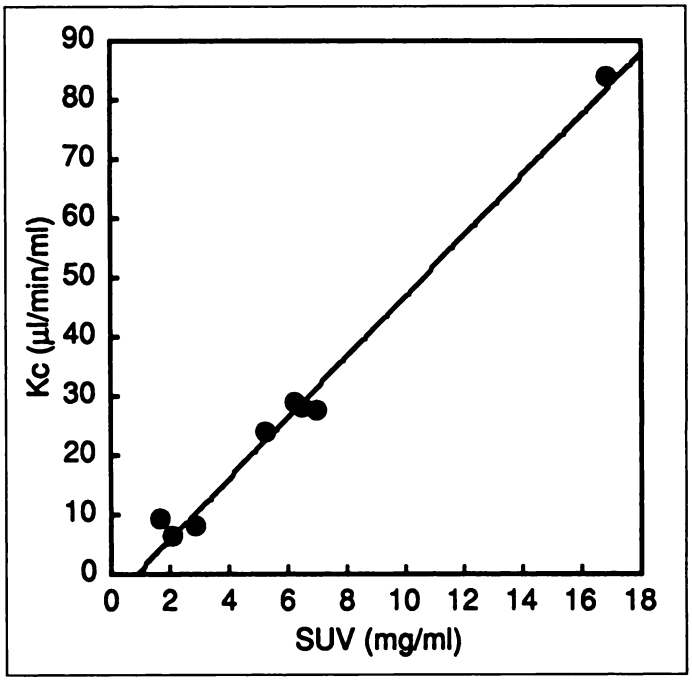

FIGURE 5. Relationship between SUV and Kc values obtained in eight patients with thyroid tumors. SUV and Kc values showed a linear correlation ($r = 0.994$).

plasma glucose levels were measured for all patients. Written informed consent was obtained from all subjects.

Thallium-201 Scintigraphy

Ten patients underwent ^{201}Tl scintigraphy. After the intravenous administration of approximately 74 MBq (2 mCi) ^{201}Tl, static planar images were obtained 5 min (early image) and 2 hr (delayed image) after the injection. A small FOV gamma camera (Starcam GE-YMS, Tokyo, Japan) with a low-energy, all-purpose collimator was used for planar imaging.

FDG-PET Data Analysis

Transaxial, sagittal and coronal FDG-PET images were inspected visually on a computer display monitor (Hewlett Packard Apollo 9000 Model 735 workstation, Palo Alto, CA). Regions of interest (ROIs) were drawn for quantification of FDG uptake on the lesions. The ROI size and anatomic location were determined on the basis of transaxial PET images, which were correlated with the anatomic location shown on CT scans. If the thyroid nodule could not definitely be identified on the FDG-PET images, large ROIs were drawn to include the nodule as determined by corresponding CT scans. The average standardized uptake values (SUVs) were calculated with the following formula:

$$SUV = \frac{\text{radioactivity in ROI (Bq/cm}^3\text{)}}{\text{injected dose (Bq)/body weight (g)}}. \qquad \text{Eq. 1}$$

The graphical analysis was performed using the same ROIs as the SUV calculation. The K complex (Kc) value was determined using the linear fitting of the time-activity curve of FDG accumulation based in the Gjedde-Patlak plot (*26,27*).

Thallium-201 Scintigraphy Image Interpretation

Accumulation of ^{201}Tl in thyroid tumors was divided into three grades on the basis of the degree of ^{201}Tl activity in the area corresponding to the nodules on CT scans compared with background activity (*11*). Delayed scanning has been reported to be useful in differentiating malignant from benign tumors (*11*); hence, in this study, only delayed images were evaluated. The groupings were as follows: a nodule with markedly increased ^{201}Tl uptake

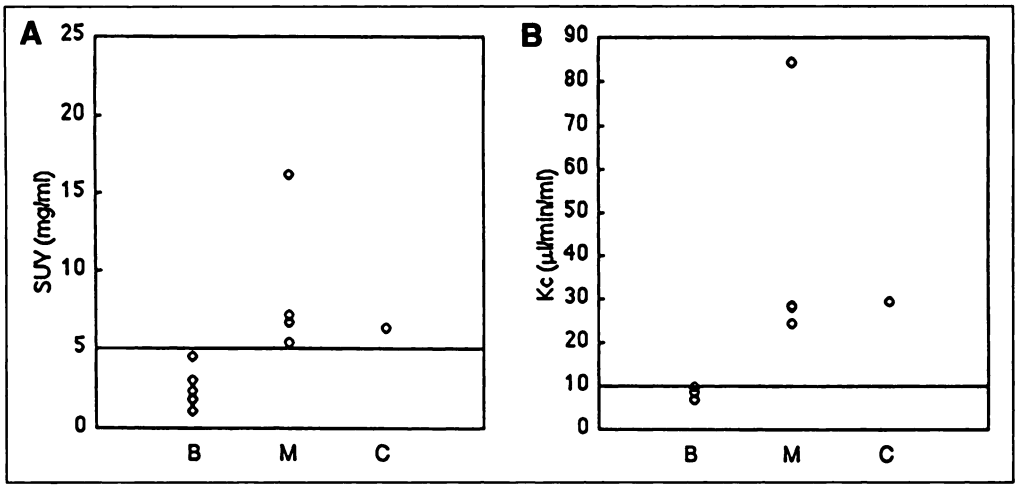

FIGURE 6. (A) Results (expressed as SUVs) for malignant lesions (n = 4), benign lesions (n = 6) and chronic thyroiditis (n = 1). B = benign; M = malignant; C = chronic thyroiditis. Scatter plot shows good separation between malignant and benign lesions. With use of a cutoff value of 5.0 mg/ml for SUV, all four of the malignant nodules and the six benign nodules were separated correctly. The SUV cutoff (5.0 mg/ml) for discrimination from malignant lesions is shown by the solid line. Chronic thyroiditis had SUVs in the malignant range. (B) Results (expressed as Kc) for malignant lesions (n = 4) and benign lesions (n = 3) and chronic thyroiditis (n = 1). Scatter plot shows good separation between malignant and benign lesions. Using a cutoff value of 10 $\mu l \cdot min^{-1} \cdot ml^{-1}$ for Kc, all four malignant nodules and the three benign nodules were separated correctly. The Kc cutoff (10.0 $\mu l \cdot min^{-1} \cdot ml^{-1}$) for discrimination from malignant lesions is shown by the solid line. Chronic thyroiditis had a Kc value in the malignant range.

compared with background activity (++), a nodule with ^{201}Tl uptake only slightly higher than or equal to background activity (+) and a nodule with ^{201}Tl uptake lower than background activity (−).

When nodules showed markedly increased ^{201}Tl uptake compared with background activity (++) in delayed images, we designated these nodules as malignant tumors.

Statistical Analysis

The Mann-Whitney U-test was used to test the hypothesis that FDG uptake was greater in malignant than benign thyroid lesions. Significance was set at the 0.05 level.

RESULTS

All patients had undergone a subtotal thyroidectomy. The final pathological diagnosis was established by surgical resection in all patients. On the basis of the histopathological results, 4 of 11 nodules were well-differentiated papillary carcinoma, and five others were benign follicular adenomas. One was a multinodular goiter, and another was a chronic thyroiditis that was proved not to contain a nodule by histopathological result. The results of FDG-PET, ^{201}Tl scintigraphy and histological examinations are summarized in Table 1.

All the malignant tumors and one nodule of the multinodular goiter were clearly identified as areas of increased FDG uptake (Figs. 1 and 2). All of the follicular adenomas and the remaining portion of the multinodular goiter could not be visualized as areas of increased FDG uptake (Figs. 2 and 3).

The time-activity curves of FDG uptake showed different patterns in malignant and benign tumors. In the malignant tumors, FDG uptake increased with time after the tracer injection (Fig. 4A). By contrast, FDG uptake of benign tumors gradually decreased (Fig. 4B).

All the malignant tumors had SUV calculated from and Kc values greater than 5.69 mg/ml and 24.0 $\mu l \cdot min^{-1} \cdot ml^{-1}$, respectively. All the benign nodules had SUV (Eq. 1) and Kc values less than 4.36 mg/ml and 9.36 $\mu l \cdot min^{-1} \cdot ml^{-1}$, respectively.

SUV and Kc values showed a positive correlation in this study (r = 0.994; Fig. 5). SUV and Kc values of the malignant

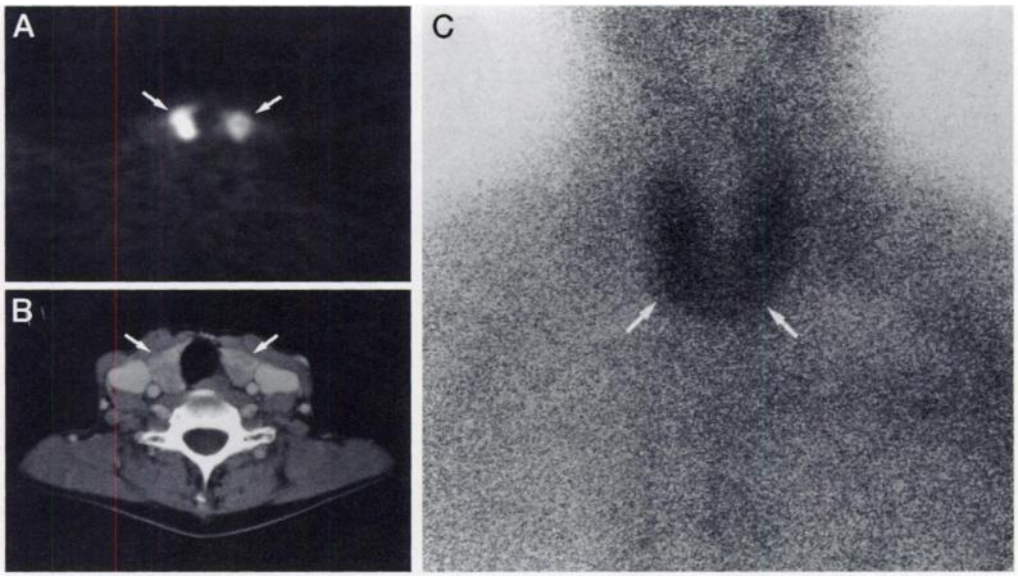

FIGURE 7. A 58-yr-old woman with chronic thyroiditis, which was suspected to contain a nodular lesion in the right lobe on clinical examination. The right lobe was resected, and it was proved not to contain a nodule. Histological diagnosis was chronic thyroiditis. (A) FDG-PET shows diffuse uptake in the thyroid (white arrows; SUV: 6.30 mg/ml, Kc: 28.73 $\mu l \cdot min^{-1} \cdot ml^{-1}$). (B) On the corresponding CT image, CT density was diffusely decreased (white arrows). (C) On the delayed ^{201}Tl scintigraphic image, ^{201}Tl uptake was moderately higher than background activity (white arrows, +).

tumors were significantly higher than that of benign thyroid tumors ($p < 0.05$, Mann-Whitney U-test).

Using a cutoff value of 5.0 mg/ml for SUV and 10 $\mu l \cdot min^{-1} \cdot ml^{-1}$ Kc (determined retrospectively), all the four malignant nodules and the six benign nodules were separated correctly, and the sensitivity and specificity of FDG-PET for differentiation of malignant from benign thyroid nodules were 100% and 100%, respectively (Fig. 6). However, chronic thyroiditis had SUV and Kc values in the malignant range (Figs. 6 and 7).

Ten patients underwent ^{201}Tl scintigraphy. In one patient with chronic thyroiditis, the delayed ^{201}Tl images revealed a diffuse accumulation higher than the background activity (+). Of the four papillary carcinomas, the delayed ^{201}Tl images revealed a moderately higher than or equal to background activity (+) in all patients. Of the follicular adenomas and multinodular goiter, the delayed ^{201}Tl images revealed a moderately higher than or equal to background activity (+) in all patients. These nine tumors were determined to be benign by preoperative ^{201}Tl image interpretation.

DISCUSSION

In the research presented here, the visual scoring method, originally proposed by Ochi et al. (*11*), was applied. Using the criterion for the malignancy as the markedly increased uptake of ^{201}Tl in delayed scan (++), they reported that the sensitivity was 46% and specificity was 100% for the detection of thyroid carcinoma. With the criterion for the malignancy as the only slightly higher than or equal to background activity (+), they reported that the sensitivity was 94.6% but that specificity was 90% for the detection of thyroid carcinoma.

In this study—of the follicular adenomas, multinodular goiter and papillary carcinoma—the delayed ^{201}Tl images revealed a moderately higher than or equal to background activity (+) in all patients. There were no tumors with markedly increased uptake of ^{201}Tl in delayed scan (++). Hence, compared with the results of FDG-PET, delayed ^{201}Tl scanning was not satisfactory in differentiating malignant from benign tumors, as previously reported (*11*). Although the results were obviously limited to the small number of patients, it is evident that FDG-PET is superior to ^{201}Tl in differentiating malignant from benign tumors.

In this study, quantitative analysis (i.e., SUV) demonstrated a significantly higher FDG uptake for malignant tumors than for benign lesions, suggesting that FDG-PET imaging may play an important role in the guidance of care for patients with thyroid nodules. Lesions demonstrating increased FDG uptake and SUV and Kc values greater than 5 mg/ml, 10 $\mu l \cdot min^{-1} \cdot ml^{-1}$ respectively, should be considered malignant. Furthermore, lesions with low uptake (i e., SUV and Kc values less than 5 mg/ml and 10 $\mu l \cdot min^{-1} \cdot ml^{-1}$, respectively) were always benign. This 100% specificity has considerable implications for patient management.

In this study, all the primary malignant tumors were pathologically well-differentiated papillary carcinoma; no aggressive poorly differentiated carcinomas were included. Brendel et al. (*28*) reported that ^{201}Tl cannot be recommended for follow-up of differentiated thyroid carcinomas because its overall sensitivity in detecting tumors is relatively poor. Therefore, FDG-PET may be helpful in detecting the differentiated carcinoma, recurring local tumors and metastases after surgery in which ^{201}Tl scans are negative.

In this study, chronic thyroiditis showed considerably increased FDG uptake. It has been reported that FDG accumulates not only in malignant tumors but also in inflammatory and infectious lesions (*29–31*). This is attributed to the increased metabolic activity in leukocytes and other cells (*29*). Pathological specimens taken in the case of chronic thyroiditis proved the existence of many infiltrating lymphocytes. This result may affect the accumulation of the FDG in the event of chronic thyroiditis. Chronic thyroiditis also was positively delineated by ^{201}Tl (*10*). Hence, researchers should confirm the laboratory values, clinical history and physical examination in case of chronic thyroiditis.

Kc values were determined from graphical analysis as originally proposed by Gjedde and Patlak (*26,27*). This index is considered to reflect tumor use of glucose, although absolute values for glucose metabolism cannot be estimated with certainty because of differences in the affinities of FDG and glucose transport and phosphorylation in generally heterogeneous malignant tissue. A good correlation between Kc and SUV values has been reported in lung cancer (*32*). Similar correlations were observed between SUV and Kc values in this study. The SUV, which is a simple parameter, provided valuable information differentiating malignant from benign tumors.

FDG-PET successfully discriminated between malignant and benign tumors. However, chronic thyroiditis showed a linear increase in FDG accumulation up to 60 min and increased FDG uptake (SUV and Kc values 6.30 mg/ml and 28.73 $\mu l \cdot min^{-1} \cdot ml^{-1}$, respectively). The overlap of SUV and the Kc values derived from the chronic thyroiditis patient signifies the problem of differentiating malignant from chronic inflammatory process.

The partial volume effect is a potential source of error in quantifying FDG activity in tissue. When the size of the ROI is smaller than about twice the full width at half maximum (FWHM), FDG activity in the ROI is underestimated. In this study, the average tumor size was relatively large (above 1.5 cm in diameter), and the FWHM of a reconstructed FDG-PET image was 4.2 mm. Hence, we could estimate the precise FDG activity in tumors. Kubota et al. (*33*) reported that in the analysis of lung tumor with FDG, malignant tumors have a higher glucose metabolic demand than benign tumors regardless of size. Hence, the criteria shown in this study would be applicable for the evaluation of smaller nodules with correction for partial volume effect.

CONCLUSION

FDG-PET discriminated malignant tumors from benign nodules. It is evident that FDG-PET is superior to ^{201}Tl in differentiating malignant from benign tumors. Both SUV and Kc values were useful indexes for this discrimination. Although careful evaluation is needed for chronic inflammatory lesions, this technique appears to be useful in evaluating thyroid nodules.

ACKNOWLEDGMENTS

We thank Teruo Matsushita, RT, Department of Radiology, Fukui Medical School, for assistance with ^{201}Tl scintigraphy data collection.

REFERENCES

1. Hopkins CR, Reading CC. Thyroid and parathyroid imaging. *Semin Ultrasound CT MR* 1995;16:279–295.
2. Feitas JE, Freitas AE. Thyroid and parathyroid imaging. *Semin Nucl Med* 1994;24: 234–245.
3. Gharib H, Goellner JR. Fine-needle aspiration biopsy of the thyroid. *Ann Intern Med* 1993;118:282–289.
4. Kusic Z, Becker DV, Saenger EL, et al. Comparison of technetium-99m and iodine-123 imaging of thyroid nodules: correlation with pathologic findings. *J Nucl Med* 1990;31:393–399.
5. Aktolum C, Bayhan H, Kir M. Clinical experience with ^{99m}Tc-MIBI imaging in patients with malignant tumors: preliminary results and comparison with ^{201}Tl. *Clin Nucl Med* 1992;17:171–176.
6. Hassan IM, Schweil A, Constantinides C, et al. Uptake and kinetics of ^{99m}Tc-hexakis

2-methoxy-isobutyl-isonitrile in benign and malignant lesions in the lung. *Clin Nucl Med* 1989;14:333–340.
7. Taillerfer R, Boucher Y, Potvin C, Lambert R. Detection and localization of parathyroid adenomas in patients with hyperparathyroidism using a single radionuclide imaging procedure with technetium-99m-sestamibi (double-phase study). *J Nucl Med* 1992;33:1801–1807.
8. O'Doherty M, Kettle AG, Wells P, Collins REC, Coakley AJ. Parathyroid imaging with technetium-99m-sestamibi: preoperative localization and tissue uptake studies. *J Nucl Med* 1992;33:313–318.
9. Nakahara H, Noguchi S, Murakami N, et al. Technetium-99m-sestamibi scintigraphy compared with thallium-201 in evaluation of thyroid tumors. *J Nucl Med* 1996;37: 901–904.
10. Tonami N, Bunko H, Michigishi T, Kuwajima A, Hisada K. Clinical application of Tl-201 scintigraphy with cold thyroid nodules. *Clin Nucl Med* 1977;2:75–81.
11. Ochi N, Sawa H, Fukuda T, et al. Thallium-201-chloride thyroid scintigraphy to evaluate benign and/or malignant nodules. *Cancer* 1982;50:236–240.
12. Koizumi M, Taguchi H, Goto M, Nomura T, Watari T. Thallium-201 scintigraphy in the evaluation of thyroid nodules: a retrospective study of 246 cases. *Ann Nucl Med* 1993;7:147–152.
13. Ramanna L, Waxman A, Braunstein G. Thallium-201 scintigraphy in differentiated thyroid cancer: comparison with radioiodine scintigraphy and serum thyroglobulin determinations. *J Nucl Med* 1991;32:441–446.
14. Laubenbacher C, Saumweber D, Wagner-Manslau C, et al. Comparison of fluorine-18-fluorodeoxyglucose PET, MRI and endoscopy for staging head and neck squamous-cell carcinomas. *J Nucl Med* 1995;36:1747–1757.
15. Lapera M, Grenman R, Kurki T, et al. Head and neck cancer: detection of recurrence with PET and 2-[F-18]fluoro-2-deoxy-D-glucose. *Radiology* 1995;197:205–211.
16. Braams JW, Pruim J, Freling NJ, et al. Detection of lymph node metastases of squamous-cell cancer of the head and neck with FDG-PET and MRI. *J Nucl Med* 1995;36:211–216.
17. Chaiken L, Rege S, Hoh C, et al. Positron emission tomography with fluorodeoxyglucose to evaluate tumor response and control after radiation therapy. *Int J Radiat Oncol Biol Phys* 1993;27:455–464.
18. Greven KM, Williams DW, Keyers JW, et al. Distinguishing tumor recurrence from irradiation sequelae with positron emission tomography in patients treated for larynx cancer. *Int J Radiat Oncol Biol Phys* 1994;29:841–845.
19. Reisser C, Habenkorn U, Dimitrakopoulou-Strauss A, et al. Chemotherapeutic management of head and neck malignancies with positron emission tomography. *Arch Otolaryngol Head Neck Surg* 1995;121:272–276.
20. Strauss LG, Conti PS. The application of PET in clinical oncology. *J Nucl Med* 1991;32;623–648.
21. Adler LP, Bloom AD. Positron emission tomography of thyroid masses. *Thyroid* 1993;3:195–200.
22. Bloom AD, Adler LP, Shuck JM. Determination of malignancy of thyroid nodules with positron emission tomography. *Surgery* 1993;114:728–735.
23. Feine U, Lietzenmayer R, Hanke JP, Held J, Wöhle H, Müller-Schauenburg M. Fluorine-18-FDG and iodine-131-iodide uptake in thyroid cancer. *J Nucl Med* 1996;37:1468–1472.
24. Grünwald F, Schomburg A, Bender H, et al. Fluorine-18-fluorodeoxyglucose positron emission tomography in the follow-up of differentiated thyroid cancer. *Eur J Nucl Med* 1996;23:312–319.
25. DeGrado TR, Turkington TG, Williams JJ, et al. Performance characteristics of a whole-body PET scanner. *J Nucl Med* 1994;35:1398–1406.
26. Patlak C, Blasberg R, Fenstermacher J. Graphical evaluation of blood-to-brain transfer constants from multiple-time uptake data. *J Cereb Blood Flow Metabol* 1983;3:1–7.
27. Gjedde A. High- and low-affinity transport of D-glucose from blood to brain. *J Neurochem* 1981;36:1463–1471.
28. Brendel AJ, Guyot M, Jeandot R, Lefort G, Manciet G. Thallium-201 imaging in the follow-up of differentiated thyroid carcinoma. *J Nucl Med* 1988;29:1515–1520.
29. Kubota R, Yamada S, Kubota K, Ishikawa K, Tamahashi N, Tatsuo I. Intratumoral distribution of fluorine-18-fluorodeoxyglucose in vivo: high accumulation in macrophages and granulation tissues studied by microautoradiography. *J Nucl Med* 1992; 33:1972–1980.
30. Lewis P, Salama A. Uptake of fluorine-18-fluorodeoxyglucose in sarcoidosis. *J Nucl Med* 1994;35:1647–1649.
31. Ichiya Y, Kuwabara Y, Sasaki M, et al. FDG-PET in infectious lesions: the detection and assessment of lesion activity. *Ann Nucl Med* 1996;10:185–191.
32. Minn H, Zasadny KR, Quint LE, Wahl RL. Lung cancer: reproducibility of quantitative measurements for evaluating 2-[F-18]-fluoro-2-deoxy-D-glucose uptake at PET. *Radiology* 1995;196:167–173.
33. Kubota K, Matsuzawa T, Fujiwara T, et al. Differential diagnosis of lung tumor with positron emission tomography: a prospective study. *J Nucl Med* 1990;31:1927–1933.

Metastatic Axillary Lymph Node Technetium-99m-MIBI Imaging in Primary Breast Cancer

Raymond Taillefer, André Robidoux, Sophie Turpin, Raymond Lambert, Jacques Cantin and Jean Léveillé
Departments of Nuclear Medicine and General Surgery, Hopital Hôtel-Dieu De Montréal, Montréal, Canada

Technetium-99m-MIBI scintimammography has been shown to be useful in the detection of primary breast cancer. The purpose of this study was to evaluate the potential role of scintimammography in detecting axillary lymph node involvement in patients undergoing scintimammography to detect primary breast cancer. **Methods:** A group of 100 women with breast cancer who were scheduled for a Level I-II axillary dissection were prospectively studied. Scintimammography was performed in all patients before histopathologic confirmation of breast cancer. Two lateral (prone imaging) views and one anterior (supine) planar thoracic view were obtained 10–15 min after the injection of 25–30 mCi ^{99m}Tc-MIBI (10 min/view) by using a special breast positioning device (foam cushion) placed over the imaging table. Both of the axilla were included in the field-of-view. Two experienced blinded observers reviewed all cases both from films and from the computer screen with contrast adjustment when needed. The site of intravenous injection of ^{99m}Tc-MIBI was known to the interpreters in order to avoid reading any false-positive uptake in the axilla ipsilateral to the injection site. **Results:** A total of 52 patients had no axillary lymph node involvement (611 negative nodes) while 48 patients had at least one axillary lymph node with metastatic involvement (180/502 positive nodes). The sensitivity of scintimammography in detecting metastatic axillary lymph node involvement was 79.2% (38/48), and the specificity was 84.6% (44/52). The positive and the negative predictive values were 82.6% (38/46) and 81.5% (44/54), respectively. **Conclusion:** This study shows that scintimammography has good diagnostic accuracy for detecting axillary lymph node involvement in patients with breast cancer. This information should be added to the result of standard scintimammography, which requires very minor modifications in order to simultaneously evaluate both of the axilla.

Key Words: technetium-99m-MIBI; breast cancer; axillary lymph nodes

J Nucl Med 1998; 39:459–464

Mammography currently represents the best imaging modality for the early detection and diagnosis of breast cancer (*1–7*). Although numerous advances and improvements in mammography have occurred, this technique is not without some drawbacks (*8–12*). Therefore, other methods to investigate the breast have been studied. These include ultrasound, MRI, CAT, digital mammography, PET and SPECT (*13–15*). Most of these methods have been developed primarily to improve the detection and diagnosis of a breast mass but not to detect metastatic axillary lymph node involvement. Since axillary lymph node involvement has been shown to be one of the most important prognostic factors for determining survival in patients with newly diagnosed primary breast cancer, almost every patient with invasive, and many with noninvasive, cancer will undergo

Received Jan. 9, 1997; revision accepted Jun. 12, 1997.
For correspondence or reprints contact: Raymond Taillefer, MD, Département de Médecine Nucléaire, Hôtel-Dieu de Montréal, 3840 St-Urbain, Montréal H2W 1T8, Canada.